A NOVEL NUMERICAL MODEL FOR THE THERMAL IMPACT OF FOUNTAINS

Fei Xue, Xiaofeng Li
Department of Building Science, Tsinghua University, Beijing, China

ABSTRACT

Fountains are delightful sceneries and can provide refreshing surrounding atmosphere, because of the cooling and humidifying effect of water droplets. To create more pleasant environment, it is valuable to quantify the thermal effect of fountains. This paper introduces a numerical fountain model based on Particle-Source-In Cell (PSI-Cell) model coupling the jet breakup process, the heat, mass and momentum transfer between droplets and air, and the CFD model of airflow, in which the influence of fountain is taken as source terms. A field measurement was conducted, where the data of one hour was selected to validate the fountain model. The presented model is proved to have good precision in the comparisons against the measured temperature and humidity. This new model is capable of estimating the trajectories of droplets, as well as the impact of fountains on the wind velocity, temperature, and humidity in the ambient area. Both the numerical and experimental results show that the fountain can improve the thermal environment in the leeward area by strong cooling and humidifying effect, while minor changes have been made in the windward and lateral areas.

INTRODUCTION

In recent years, deterioration of outdoor environment caused by heat island effect and similar phenomenon has become an increasingly serious problem for urban areas (Arnfield, 2003). The heat island intensity can result in as much as 10 ˚C temperature difference between the dense urban area and the surrounding rural zones (Santamouris et al., 2001). Put together with the effects of the intensive solar radiation and the heat radiating from surrounding buildings, the high temperature makes the thermal environment in urban areas extremely uncomfortable in summers.

In order to analyze the urban microclimate, numerous studies were carried out. Among the strategies proposed to improve the urban microclimate, evaporative cooling is arguably one of the most efficient ways of passive cooling for urban spaces in hot regions (Givoni, 1991; Ken-Ichi, 1991). The provisions of water facilities, such as ponds, fountains, sprays, and canals, are important countermeasures that ease the microclimate some. Most researches on water facilities focused on urban water bodies, such as rivers, canals, ponds and lakes. A field experiment on a small lake in Israel showed that the air temperature at leeward of the lake was 0.9-1.6 K lower than at windward, during noon both in hot dry and sultry days (Saaroni and Ziv, 2003). Similar results were also obtained by other experiments on water ponds and lakes (Givoni and La Roche, 2000; Lin and Matzarakis, 2008).

Compared with the amount of studies made on water ponds (Inard et al., 2004; Robitu et al., 2003), research on fountains is even less. Nishimura et al. (Nishimura et al., 1998) proposed novel water facilities, including fountains, to make the most efficient use of water's ability to adjust temperature and humidity. For verification, a field measurement and wind tunnel experiment were conducted in their study. However, despite that numerical models for water spray evaporation in buildings have been proposed (Belarbi et al., 2006; Kachhwaha et al., 1998), no numerical study on fountains has been published, which is a deficiency in urban microclimate research. In order to acquire a better understanding of the beneficial phenomenon of fountains and make it effective in practical applications, the research in fountains still needs further improvement in numerical models.

For this purpose, based on the investigation of the jet breakup process and interactions between droplets and air, this paper presents the development of a numerical model, which allows the evaluation of the impact of fountains on the urban microclimate and the comfort of pedestrians. A field measurement on the cooling and humidifying effect of a fountain was also carried out to validate the proposed model.

NUMERICAL MODELLING

A fountain influences the ambient environment mainly by the interaction (heat, mass, and momentum transfer) between the sprayed droplets and air. Therefore, in order to build a proper model for the fountains, there are three aspects that should be investigated: (1) jet breakup process, (2) heat, mass, and momentum transfer between droplets and air and (3) calculation approach for coupling of droplets and air flow.

Jet breakup process

The breakup process determines the initial conditions of all the sprayed droplets, which are essential in the

following simulation process. Therefore, in order to determine the onset of breakup, diameter and velocity distributions after the breakup, the jet breakup process should be investigated further. After the water has been sprayed out, it becomes a water column near the nozzle. The adhesive force and decomposition force both exist on the surface of the water column and cause shaking and perturbation (Faeth et al., 1995). Under proper condition, the oscillation is amplified and the droplets are discomposed from the water column. This process is called primary breakup. If the droplet diameter is larger than the critical value, it will continue splitting into smaller droplets. This stage is called the secondary breakup and will stop breaking up and remain the sizes with a decreasing velocity and increasing height.

The whole process is too complicated to emulate perfectly with numerical method. Therefore, the breakup process was simplified as an abrupt change, assuming that the jet water completely split up at the onset of breakup. The correlation between the jet breakup length (i.e. the distance between the onset of breakup and the jet exit) and the nozzle diameter was developed by Grant and Middleman(Grant and Middleman, 1966), based on both their measurements and those of Chen and Davis (Chen and Davis, 1964) defined as

$$l = 8.51 D We_{LD}^{0.32} \quad (1)$$

where l is the breakup length, D is the nozzle diameter, $We_{LD}=\rho_L \bar{u}_0^2 D/\sigma$ is the jet exit Weber number, ρ_L is the liquid density, $\bar{u}_0$ is the jet exit mean velocity and σ is the surface tension. Eq. (1) was proved to be practical in a sufficient We_{LD} range after being analyzed and compared with other correlations by Sallam et al. (Sallam et al., 2002).

After the fully completed breakup as assumed, the water column is atomized into droplets with different sizes and velocities, and the distribution function is an efficient method to describe the droplet size and velocity. Past studies (Hsiang and Faeth, 1992, 1993; Ruff et al., 1992; Tseng et al., 1992; Wu and Faeth, 1993; Wu et al., 1992; Wu and Faeth, 1995) have shown that the measured size distributions of droplets for both primary and secondary breakup processes satisfied the universal root normal distribution function, with *MMD/SMD* = 1.2, due to Simmons (Simmons, 1977), where *MMD* denotes the mass median diameters of the droplet size distributions and *SMD* is the Sauter mean diameter, which can be considered as the diameter of a drop having the same volume/surface area ratio as the entire spray, and is defined as

$$SMD = \frac{\Sigma_{i=1}^{n} d_i^3}{\Sigma_{i=1}^{n} d_i^2} \quad (2)$$

where n is the number of drops in the distribution and d_i is the diameter of the drop i in a drop distribution. The constant *MMD/SMD* ratio vastly simplifies the prediction of the size distributions, because the universal root normal distribution function has only two moments. As such, with *MMD/SMD* = 1.2, the distribution can be entirely described by the *SMD* alone.

In the fountain model, the *SMD* after the breakup process is calculated according to the best fit correlation of merged primary and secondary breakup made by Faeth et al. (Faeth et al., 1995) as follows

$$\rho_G SMD \bar{u}_0^2/\sigma = 12.9\left(x/\Lambda\right)^{1/3}\left(\rho_G/\rho_L\right)^{3/4} We_{L\Lambda}^{5/6} Re_{L\Lambda}^{-1/2} \quad (3)$$

where ρ_G and ρ_L denote the gas density and liquid density, respectively, Λ is the radial integral length scale of the turbulence, which is taken to be *D/8*, based on Laufer's measurements (Hinze, 1975), $We_{L\Lambda}=\rho_L \Lambda \bar{u}_s^2/\sigma$, $Re_{L\Lambda}=\rho_L \Lambda \bar{u}_s/\mu_L$, μ_L is the liquid viscosity and $\bar{u}_s$ is the time-averaged local streamwise liquid surface velocity, which is approximately equals to $\bar{u}_0$ (within 10%), according to Wu and Faeth (Wu and Faeth, 1995). Therefore, $\bar{u}_s=\bar{u}_0$ was adopted in the fountain model.

The droplet velocity distribution is another important parameter. Earlier findings by Sallam et al. (Sallam et al., 1999, 2002) showed that the droplet velocity distributions after turbulent primary breakup were essentially uniform. Thus, the droplet velocities is reported as time-averaged absolute streamwise and cross stream velocities normalized by the jet exit mean velocity, $\bar{u}_p/\bar{u}_0$ and $\bar{v}_p/\bar{u}_0$, as follows

$$\bar{u}_p/\bar{u}_0 = 0.89,\ \bar{v}_p/\bar{u}_0 = 0.04 \quad (4)$$

With the parent droplet velocities defined after primary breakup, the correlation between droplet sizes and velocities after breakup process (both primary and secondary) was used to obtain the final velocity distribution. This was done by adopting the correlation proposed by Hsiang and Feath (Hsiang and Faeth, 1993), yielding to

$$\bar{u}_0/\bar{u}_d - 1 = 2.7\left[\left(\rho_G/\rho_L\right)^{1/2} d_0/d\right]^{1/2} \quad (5)$$

where $\bar{u}_d$ is the mean velocity of droplets having diameter d at the end of the breakup process, and d_0 is the initial diameter in the secondary breakup stage. For a certain diameter, the velocity distribution agrees to the normal distribution, and the experimental data indicated that the dimensionless droplet velocity range was 0.5~1.5 (Kachhwaha et al., 1998). However, under the influence of ambient air flow, droplet velocity would practically be identical. Therefore, it is reasonable to adopt an equal after breakup velocity for the droplets with the same size, as we did in the fountain model.

After the calculation of the jet breakup process, the results of the breakup onset, diameter distribution and velocity distribution are adopted as the initial jet

conditions in the following simulation to calculate the interaction between the droplets and air.

Heat, mass, and momentum transfer between droplets and air

The fundamental process is the heat and mass transfer between droplets and air, which has been extensively investigated in past work. Some assumptions are summarized here (Godsave, 1953; Spalding, 1953): (1) Droplets are a hard sphere. (2) Radiation transfer between droplets and surrounding objects is ignored. (3) Water vapor and air are treated as ideal gas. (4) Droplets' Bi is less than 0.1 and it can be treated by lumped parameter method. (5) The air on the surface of the droplet is saturated and has the same temperature as the droplet.

A quasi-steady state vaporization needs to be considered, which is found to be accurate enough (Lefebvre, 1988). As such, the assumptions above allow the rate of droplet vaporization to be expressed as (Chin and Lefebvre, 1983)

$$\frac{\mathrm{d}m_p}{\mathrm{d}t} = 2\pi d k_m c_{pm} \ln(1 + B_M) \tag{6}$$

where m_p is the droplet mass, t is the time, so $\mathrm{d}m_p/\mathrm{d}t$ is the rate of droplet vaporization, d is the droplet diameter, k_m is the moist air thermal conductivity, c_{pm} is the specific heat of the moist air, and B_M is the mass diffusion transfer number, which is defined as

$$B_M = (Y_{v,s} - Y_{v,\infty}) / (1 - Y_{v,s}) \tag{7}$$

where $Y_{v,s}$ is the vapor mass fraction at the droplet surface, and $Y_{v,\infty}$ is the ambient vapor mass fraction (usually equals zero).

According to the heat balance equation for the droplet (Chen and Pereira, 1996), the change in droplet temperature is given by

$$\frac{\mathrm{d}T_p}{\mathrm{d}t} = \frac{\pi D_p N u k_m (T_G - T_p)}{m_p c_{pp}} - \frac{L}{m_p c_{pp}} \frac{\mathrm{d}m_p}{\mathrm{d}t} \tag{8}$$

where T_p is the droplet temperature, Nu is the Nusselt number, T_G is the gas temperature, L is the droplet latent heat of vaporization and c_{pp} is the specific heat of the droplet (i.e. the water specific heat).

By integrating Eq. (6) and Eq. (8), the droplet mass and temperature change along the trajectory can be obtained.

The trajectory can be calculated by performing integration on droplet velocity, which can be obtained according to the momentum equation as

$$m_p \frac{d\vec{U}_p}{dt} = \frac{1}{2} \rho_L A_p C_D \left|\vec{U} - \vec{U_P}\right| (\vec{U} - \vec{U}_P) + m_p b g - V_p \nabla P \tag{9}$$

where Saffman force and Magnus force are ignored due to the small air velocity gradient (Crowe et al., 1977), $\vec{U}_p$ is the droplet velocity, $\vec{U}$ is the air velocity, A_p is the projection area of the droplet, b is the buoyancy coefficient ($=1-\rho_G/\rho_L \approx 1$), g is the gravitational acceleration, V_p is the droplet volume, ∇P is the air pressure gradient which is taken to be 0 due to the small ρ_G / ρ_L, and C_D is the drag coefficient, which is determined by (Wallis, 1969)

$$\begin{gathered} Re \le 1000,\ C_D = 24(1+0.15Re^{0.687})/Re; \\ Re > 1000,\ C_D = 0.44 \end{gathered} \tag{10}$$

where Re is the Reynolds number.

In the fountain model, an optional stochastic turbulence model is adopted to emulate the effects on particle dispersion of the turbulent fluctuations of the continuous-phase velocity. This method came from Gosman and Ioannides (Gosman and Ioannides, 1983), Shuen, et al. (Shuen et al., 1985), and Gauvin et al. (Gauvin et al., 1975). As such, the trajectory of the droplet is obtained.

Coupling calculation of the airflow and droplets

In this research, two-way coupling between air and droplet is simulated by Particle-Source-In Cell (PSI-Cell) model (Crowe et al., 1977). The main idea is to treat the effects of droplets on air as the source terms in energy, mass, and momentum equations of air phase. The airflow field is simulated by solving differential equations in the Eulerian approach. When a droplet moves through cells, it is traced along its trajectory. The droplet temperature and diameter is calculated by performing integration on the dynamic equations, and as such, the energy, mass, and momentum source of the droplet in each cell can be obtained. This idea is firstly proposed by Migdal and Agosta (Migdal and Agosta, 1967).

The flow of the gas phase is simulated by the Eulerian equation as follow:

$$\frac{\partial}{\partial t}(\rho_G \varphi_G) + \nabla \cdot (\vec{U}_G \rho_G \varphi_G) - \nabla \cdot (\Gamma \nabla \varphi_G) = S_\varphi + S_{\varphi p} \tag{11}$$

where φ_G is the parameter of the simulated gas; ρ_G is the gas density; $\vec{U}_G$ is the velocity of the gas; Γ is the interphase exchange coefficient; $S\varphi$ is the source or the sink of φ_G; $S\varphi_p$ is the source term of φ_G generated by the droplets.

Specifically in the fountain model, firstly, the initial airflow field was simulated without droplets using CFD (Computational Fluid Dynamics) method. Then, in the simulated airflow field, the droplet trajectories, diameters and temperature changes were calculated. With these data, the energy, mass, momentum source terms of the droplets in every cell could be obtained, which were added to the corresponding conservation equations to calculate the new airflow field. The new airflow field is used to calculate the new droplet trajectory, diameter and temperature. This iteration procedure would be repeated until convergence was reached. As such, the coupling calculation between the airflow and droplets was completed.

FIELD MEASUREMENT

A field measurement was conducted in Beijing in August to validate the theoretical model. An overland fountain on an open field was selected as Fig. 1. The spray nozzles were arranged by 5 × 9, with 3.4 m intervals lengthways and 1.7 m breadthways. Each nozzle was made up of 6 small vertical pipes, with a diameter of 9.5 mm, spraying water continuously. The water flowed back to an underground tank through sewers. The fountain was settled in a wide open area, with no buildings in 40 m in the east and west direction and over 100 m in the south and north direction. The ground was covered by grass, with only a few small trees with little leaves and some narrow marble paths in the surroundings.

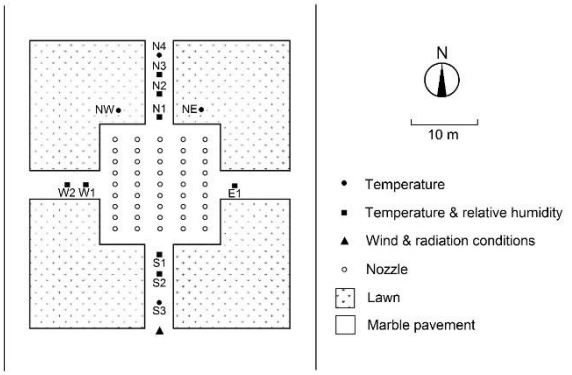

Figure 1 The measurement field and test points

Test points arrangement

As shown in Fig. 1, there were 8 test points monitoring both dry bulb temperature and relative humidity and 4 test points only for dry bulb temperature. All of the 12 test points were positioned 1.5 m above ground (pedestrian level), considered to be the most reasonable height for outdoor thermal environment study. One additional temperature sensor was positioned on a water pipe wall near the nozzle to monitor the water temperature. Besides, ambient wind conditions and solar radiation intensity were measured by a hot-sphere anemometer, wind vane and pyranometer located at 6 m above the ground in the south of the fountain, due to the dominant south wind in the test day.

SIMULATION SETTINGS

The simulation was performed using the Simulation Platform for Outdoor Thermal Environment (SPOTE) (Lin et al., 2008; Ma et al., 2012), which has been validated in numerous applications including cases with two-phase flow. The standard k–ε turbulence model was used in the airflow model since previous studies have suggested that the standard k–ε turbulence model is suitable for urban street scale airflow modelling among several widely-used k–ε turbulence models (Ji and Zhao, 2014). A computer code was developed to load the airflow field and calculate the droplet trajectories, diameters and temperature changes using a time interval of 0.05 s. Then the energy, mass, momentum source terms of the droplets in every cell could be obtained. The property formulas of air, water and vapor were added into the code. Evaporating droplet model with stochastic turbulence was used, while droplet rebound and breakup on the ground were not considered.

During the measurement, the wind speed and direction were not steady. In order to validate the numerical method, the data of a relatively stable period from 12:30 to 13:30 was adopted in the validation.

Treatment of surroundings

The fountain is located at an open area and surrounded by lawn. Therefore an open flow with lawn ground was considered in the simulation. Heat and mass transfer between lawn and ambient air was calculated by the former mentioned validated code SPOTE (Lin et al., 2008; Ma et al., 2012).

Meteorological conditions

As the measurement data indicated, the average dry bulb temperature was 32.7˚C and average absolute humidity was 14.9 g/kg dry air, and the water temperature was set at 24.5˚C. The effect of radiation, including solar radiation and long wave radiation from the surrounding objects, on the droplets was limited. As such, radiation heat transfer was only considered in the wind field calculation and was neglected in the droplet modeling.

In the measurement period from 12:30 to 13:30, the wind speed and direction was summarized in Table 1. The wind speed and direction conditions would have great impact on the simulation results. In order to reduce the workload, the wind conditions in the simulation were simplified as five weighted wind directions with a time-averaged wind speed so that five simulations would suffice. The time-averaged wind speed, 2.9 m/s, was taken to be the inlet speed at the reference height, which was 6 m above the ground (i.e. the measurement height). Five wind directions (SE, SSE, S, SSW, and SW) were simulated and results were averaged according to the corresponding weight (the direction frequency ratio) in Table 1.

Table 1

Wind speed and direction distribution

Speed range (m/s)	<2.0	2.0-3.0	3.0-4.0	4.0-5.0	>5.0
Speed frequency ratio	13.5%	45.9%	27.0%	10.8%	2.7%
Wind direction	SE	SSE	S	SSW	SW
Direction frequency ratio	15%	20%	50%	10%	5%

Abbreviations: SE: Southeast, specifically 135˚; SSE: South-southeast, 157.5˚; S: South, 180˚; SSW: South-south west, 202.5˚; SW: Southwest, 225˚.

Initial jet velocity

The initial jet velocity at the nozzle orifice was estimated according to the spray height of the jet. The

velocity of large droplets was almost equal to the initial jet velocity and the gravity was the major factor deciding its vertical height. As such, based on the height of spout (approximately 3.95 m) the initial jet velocity was calculated as 9.9 m/s. The jet breakup was heading towards all directions, which was simplified as four directions (i.e. N, S, E, and W).

Initial droplet conditions

The droplet initial diameter and velocity distribution were obtained according to Eq. (3) and Eq. (5), respectively. The *MMD* was 1.8 mm. The droplet diameter range in the simulation was set from 0.15 mm to 5.29 mm, which covered 99.74% of the total droplet mass. Five representative droplets were adopted as the simplification of all the drops. In order to maintain the cooling and humidifying effect, *SMD*s of each interval were used as the representative diameters, as shown in Table 2. The number of each representative droplet was calculated by counting all the droplets in the corresponding interval. Fig. 4 depicts the initial mass and number distributions of the droplets.

Table 2
Division of initial droplet diameter ranges
(Unit: mm)

Interval	Lower boundary	Upper Boundary	Representative diameter
1	0.15	1.18	0.48
2	1.18	2.21	1.44
3	2.21	3.24	2.41
4	3.24	4.26	3.37
5	4.26	5.29	4.33

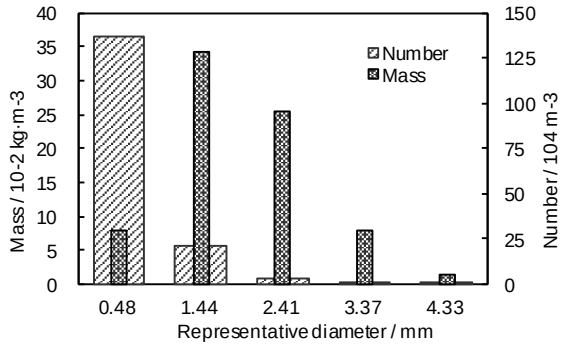

Figure 4 Initial mass and number distributions of droplets

SIMULATION RESULTS

Airflow field

The simulations with five directions were done, and the results were averaged according to the corresponding weight. The results of different wind directions was similar, therefore in this paper, the results are presented for only one wind direction, the south. The airflow field was assessed at pedestrian level (1.5 m above ground). The wind speed was slightly deduced in the leeward area. The deduction was less than 0.6 m/s, which means the influence on wind field is small.

Temperature and absolute humidity

The outdoor thermal environment was also assessed at pedestrian level. By subtracting the ambient values from the simulation results, the contoured graphs of the difference values of the dry bulb temperature and absolute humidity are illustrated in Fig. 5 (a) and (b), respectively. In the leeward area, obvious cooling effect is indicated, with a generally 1.0 to 4.0 ˚C temperature reduction. Accordingly, humidifying effect is also evident in the leeward area, where the increment of the absolute humidity is approximately between 1.0 to 4.0 g/kg dry air. The effect of the fountain can could be felt over 40 m away from the fountain, which is about ten times the height of spout. The simulation results reconfirm the cooling and humidifying effect of the fountain on the leeward area.

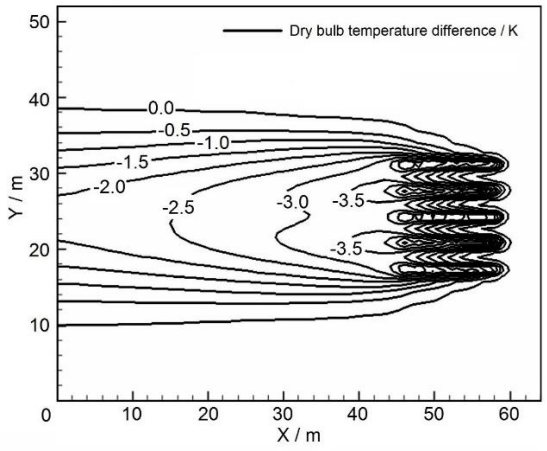

(a) Dry bulb temperature

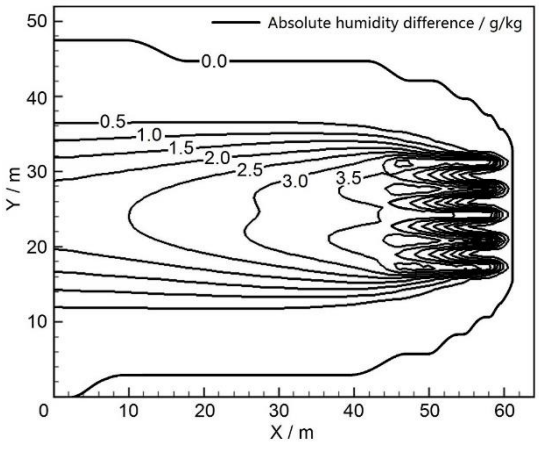

(b) Absolute humidity

Figure 5 Differences between simulated results and ambient values at Z = 1.5 m level

Droplet trajectories

Fig. 6 (a) and (b) depicts the elevation and top plan views, respectively, of the droplet trajectories after spouting out from one nozzle. The water column breaks up at about 0.4 m, after the breakup there are 20 different trajectories, which are composed of 5 kinds of droplets with different sizes in each of the four directions. For the largest droplets, the max height is about 4.2 m due to the small air drag force, while the horizontal range is only about 1.5 m. However, the air drag force has greater influence on smaller droplets, which float as far as 2.5 m away from the nozzle. As stochastic turbulence model is adopted in the simulation, the trajectories of small droplets are random.

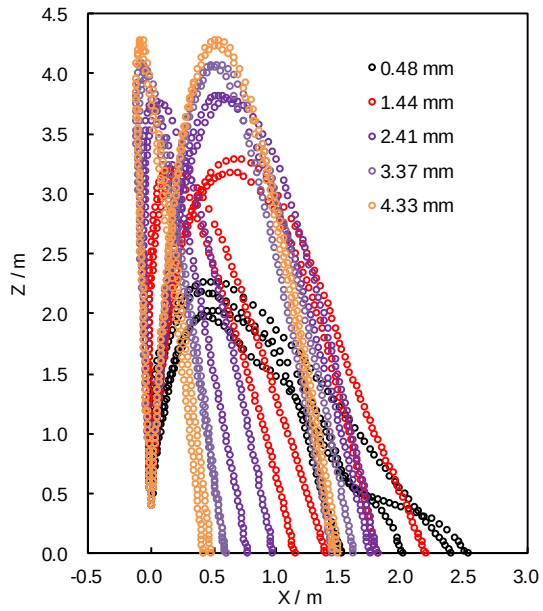

(a) Elevation view

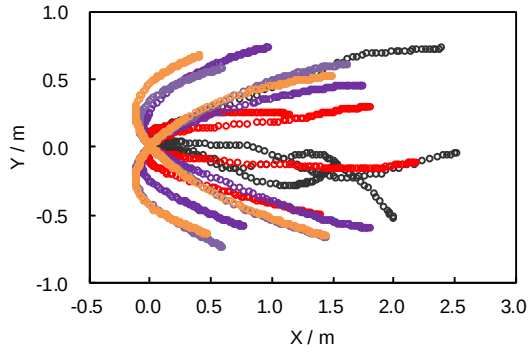

(b) Top plan view

Figure 6 Droplet trajectories from one nozzle

VALIDATION AND DISCUSSION

The average simulation results of temperature and absolute humidity were compared with the measurement data, which is averaged from 12:30 to 13:30. The comparisons of dry bulb temperature and absolute humidity for each test point are summarized in Fig. 7 (a) and (b), respectively. The absolute temperature deviations between simulated and measured results are less than 0.7 ˚C for all the test points except E1, for which is 1.4 ˚C. Although the temperature deviations are relatively small, it can be found that the temperature is generally higher in the windward and lateral areas, lower in the leeward area comparing with the measured data, indicating errors in the methodology. As for the absolute humidity, the deviations are within 0.5 g/kg in the windward and lateral areas, while in the leeward area the simulation results are about 2 g/kg higher than the field measurement data. In spite of these shortcomings, the simulation results of the presented fountain model show good correspondence with the measured temperature and humidity.

The validation also indicates the existence of method errors. Based on the comparisons, the humidifying effect of the fountain is overestimated as well as the cooling effect, accordingly, although not as rough as the former. Since the wind conditions have a great impact on the distribution of both temperature and humidity, it can be argued that the deviations are brought by the simplified wind directions and time-averaged speed. However, the wind speed in the sample time (12:30 to 13:30) was steady enough for an outdoor environment, ranged in 2.9±1.0 m/s in over 75% of the time. Besides, the deviations brought by simplified wind conditions can only be eliminated by using real-time wind conditions, which is not practical in simulations.

Another possible reason might be the deviations caused by the lawn, which was another evaporation source in the ambient. However, according to the past experimental results, the cooling effect of exposed lawn during daytime at 1.5 m level was 0.3 K, and no humidity increase was observed at 1.5 m level (Shashua-Bar et al., 2009). Compared with the fountain, the thermal impact of the lawns is negligible, especially on humidity, so that lawn model is not the main cause of the deviations.

Therefore, the deviations are probably caused by omission of the droplet collision and coalescence. For a real fountain, when the droplet trajectories intersect with each other due to the gravity and wind, droplet collision and coalescence will happen, which lead to larger droplets and weaker humidifying and cooling effect. However, to calculate the collision and coalescence, much more trajectories would be required, huge extra calculation would be added in every iteration, and the worst case could be that the coupling calculation probably comes to a divergence because the airflow field and the trajectories would have much stronger influence on each other. As such, no collision or coalescence is considered in the fountain model, and so are the deviations explained.

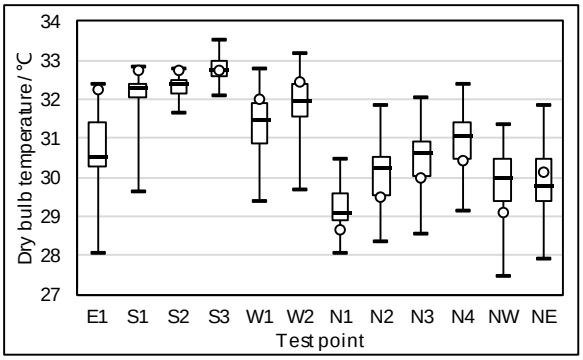

(a) Dry bulb temperature

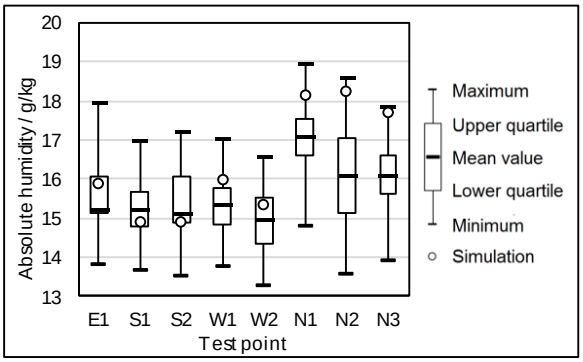

(b) Absolute humidity

Figure 7 Comparisons of simulated and measured results of each test point

CONCLUSIONS

The fountain model which was presented is capable of calculating the thermal environment around fountains by adopting PSI-Cell model combined with CFD method of airflow, the jet breakup process and the heat, mass, and momentum transfer between droplets and air. This new model can be useful for city planning and for the analysis of urban microclimate since it is capable of providing the wind velocity, temperature, and humidity in the ambient area, as well as the trajectories of droplets.

A field measurement was conducted. The measured data of one hour was used to validate the fountain model. The simulation results of the presented fountain model shows good correspondence with the measured temperature and humidity.

The humidifying effect is overestimated by the fountain model according to the validation, leading to overshoots in the leeward area. The deviations are mainly caused by the omission of the droplet collision and coalescence. In spite of the shortcomings, this modeling approach may provide useful quantitative information for fountain design decisions. Both the field measurement and the simulation results indicate that the fountains should be considered as real means for improvement of urban microclimate conditions.AcknowledgEment

This document is a summary of various documents from previous Building Simulation Conferences.

REFERENCES

Arnfield, A.J., 2003. Two decades of urban climate research: A review of turbulence, exchanges of energy and water, and the urban heat island. International Journal of Climatology 23, 1-26.

Belarbi, R., Ghiaus, C., Allard, F., 2006. Modeling of water spray evaporation: Application to passive cooling of buildings. Solar Energy 80, 1540-1552.

Chen, T.F., Davis, J.R., 1964. Disintegration of a turbulent water jet. Journal of the Hydraulics Division 90, 175-206.

Chen, X.Q., Pereira, J.C.F., 1996. Computation of turbulent evaporating sprays with well-specified measurements: A sensitivity study on droplet properties. International Journal of Heat and Mass Transfer 39, 441-454.

Chin, J.S., Lefebvre, A.H., 1983. Steady-state evaporation characteristics of hydrocarbon fuel drops. AIAA Journal 21, 1437-1443.

Crowe, C.T., Sharma, M.P., Stock, D.E., 1977. The particle-source-in cell (PSI-CELL) model for gas-droplet flows. Transactions of the ASME. Series I, Journal of Fluids Engineering 99, 325-332.

Faeth, G.M., Hsiang, L.P., Wu, P.K., 1995. Structure and breakup properties of sprays. International Journal of Multiphase Flow 21, 99-127.

Gauvin, W., Katta, S., Knelman, F., 1975. Drop trajectory predictions and their importance in the design of spray dryers. International Journal of Multiphase Flow 1, 793-816.

Givoni, B., 1991. Impact of planted areas on urban environmental quality - a review. Atmospheric Environment Part B-Urban Atmosphere 25, 289-299.

Givoni, B., La Roche, P., 2000. Indirect evaporative cooling with an outdoor pond, Architecture, City, Environment, PLEA 2000, Cambridge, UK, pp. 310-311.

Godsave, G., 1953. Studies of the combustion of drops in a fuel spray-the burning of single drops of fuel, Fourth Symposium (International) on Combusion. Elsevier, Combustion Institute, Baltimore, US, pp. 818-830.

Gosman, A.D., Ioannides, E., 1983. Aspects of computer-simulation of liquid-fueled combustors. Journal of Energy 7, 482-490.

Grant, R.P., Middleman, S., 1966. Newtonian jet stability. AIChE Journal 12, 669-678.

Hinze, J., 1975. Turbulence, 2nd ed. McGraw-Hill, New York.

Hsiang, L.P., Faeth, G.M., 1992. Near-limit drop deformation and secondary breakup. International Journal of Multiphase Flow 18, 635-652.

Hsiang, L.P., Faeth, G.M., 1993. Drop properties after secondary breakup. International Journal of Multiphase Flow 19, 721-735.

Inard, C., Groleau, D., Musy, M., 2004. Energy balance study of water ponds and its influence on building energy consumption. Building Services Engineering Research and Technology 25, 171-182.

Ji, W., Zhao, B., 2014. Numerical study of the effects of trees on outdoor particle concentration distributions. Building Simulation 7, 417-427.

Kachhwaha, S.S., Dhar, P.L., Kale, S.R., 1998. Experimental studies and numerical simulation of evaporative cooling of air with a water spray .1. Horizontal parallel flow. International Journal of Heat and Mass Transfer 41, 447-464.

Ken-Ichi, K., 1991. Evaporative cooling effects in hot and humid urban spaces, Architecture and Urban Space, Ninth International PLEA Conference, Seville, Spain, pp. 631–636.

Lefebvre, A., 1988. Atomization and sprays. CRC press.

Lin, B., Li, X., Zhu, Y., Qin, Y., 2008. Numerical simulation studies of the different vegetation patterns' effects on outdoor pedestrian thermal comfort. Journal of Wind Engineering and Industrial Aerodynamics 96, 1707-1718.

Lin, T.-P., Matzarakis, A., 2008. Tourism climate and thermal comfort in Sun Moon Lake, Taiwan. International Journal of Biometeorology 52, 281-290.

Ma, J., Li, X., Zhu, Y., 2012. A simplified method to predict the outdoor thermal environment in residential district. Building Simulation 5, 157-167.

Migdal, D., Agosta, V.D., 1967. A source flow model for continuum gas particle flow. Transactions of the ASME. Series E, Journal of Applied Mechanics 34, 860-865.

Nishimura, N., Nomura, T., Iyota, H., Kimoto, S., 1998. Novel water facilities for creation of comfortable urban micrometeorology. Solar Energy 64, 197-207.

Robitu, M., Musy, M., Groleau, D., Inard, C., 2003. Thermal radiative modelling of water pond and its influences on microclimate, Proceedings of Fifth International Conference on Urban Climate, Lodz, Poland, pp. 289-292.

Ruff, G.A., Wu, P.K., Bernal, L.P., Faeth, G.M., 1992. Continuous-phase and dispersed-phase structure of dense nonevaporating pressure-atomized sprays. Journal of Propulsion and Power 8, 280-289.

Saaroni, H., Ziv, B., 2003. The impact of a small lake on heat stress in a Mediterranean urban park: the case of Tel Aviv, Israel. International Journal of Biometeorology 47, 156-165.

Sallam, K.A., Dai, Z., Faeth, G.M., 1999. Drop formation at the surface of plane turbulent liquid jets in still gases. International Journal of Multiphase Flow 25, 1161-1180.

Sallam, K.A., Dai, Z., Faeth, G.M., 2002. Liquid breakup at the surface of turbulent round liquid jets in still gases. International Journal of Multiphase Flow 28, 427-449.

Santamouris, M., Papanikolaou, N., Livada, I., Koronakis, I., Georgakis, C., Argiriou, A., Assimakopoulos, D.N., 2001. On the impact of urban climate on the energy consumption of buildings. Solar Energy 70, 201-216.

Shashua-Bar, L., Pearlmutter, D., Erell, E., 2009. The cooling efficiency of urban landscape strategies in a hot dry climate. Landscape and Urban Planning 92, 179-186.

Shuen, J.S., Solomon, A.S.P., Zhang, Q.F., Faeth, G.M., 1985. Structure of particle-laden jets - measurements and predictions. AIAA Journal 23, 396-404.

Simmons, H., 1977. The Correlation of Drop-Size Distributions in Fuel Nozzle Sprays. Journal for Engineering for Power 99, 309-319.

Spalding, D.B., 1953. The combustion of liquid fuels, Fourth Symposium (International) on Combusion. Elsevier, Combustion Institute, Baltimore, US, pp. 847-864.

Tseng, L.K., Ruff, G.A., Faeth, G.M., 1992. Effects of gas-density on the structure of liquid jets in still gases. AIAA Journal 30, 1537-1544.

Wallis, G.B., 1969. One-dimensional two-phase flow. McGraw-Hill, New York.

Wu, P.-K., Faeth, G., 1993. Aerodynamic effects on primary breakup of turbulent liquids. Atomization and Sprays 3, 265-289.

Wu, P.-K., Tseng, L.-K., Faeth, G., 1992. Primary breakup in gas/liquid mixing layers for turbulent liquids. Atomization and Sprays 2, 295-317.

Wu, P.K., Faeth, G.M., 1995. Onset and end of drop formation along the surface of turbulent liquid jets in still gases. Physics of Fluids 7, 2915-2917.